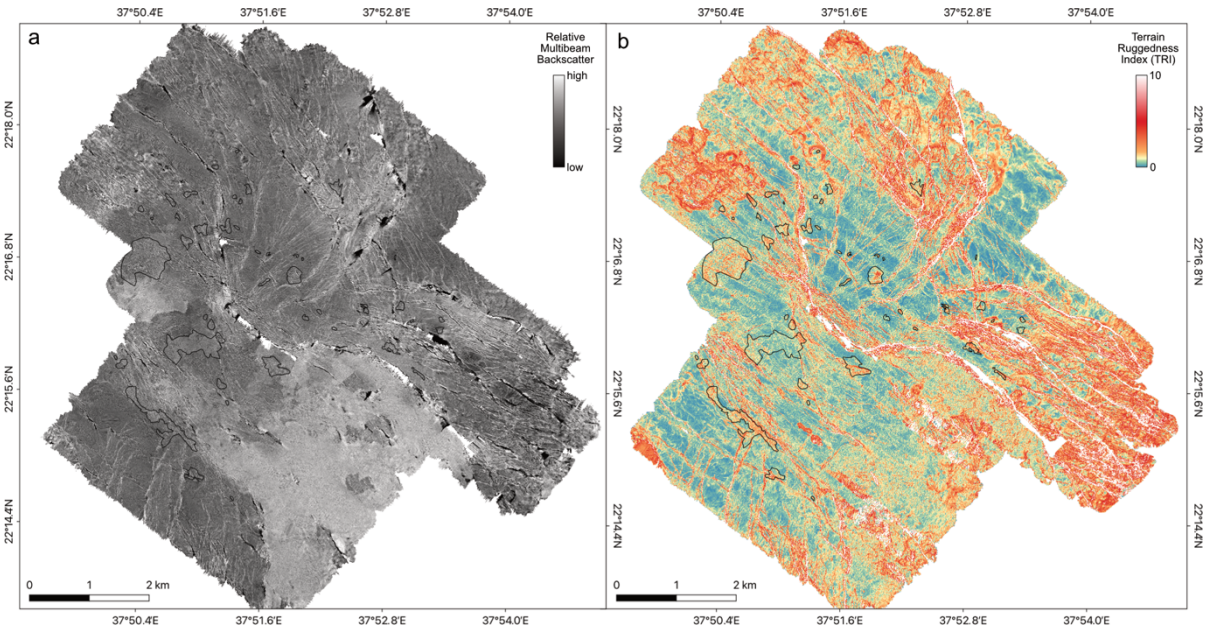

Supplementary Figure 1 - (a) AUV multibeam backscatter mosaic (1 m spatial resolution) of the summit of Hatiba Mons volcano. Low backscatter areas (smooth surface, highly sedimented) are shown in dark and high backscatter areas (rough surface, low- or no sediment) are in bright tones. The complex network of faults and fissures is highly visible in the mosaic. The youngest lava is primarily present in the rift axis (see also Figure 2 in the main text). The high-resolution backscatter mosaic is available for download from the Pangaea repository https://doi.pangaea.de/10.1594/PANGAEA.956871 **(b)** Terrain ruggedness index of AUV data from Hatiba Mons. The areas with the highest TRI at relatively large scales are caused by the volcanic mounds in the central valley and the most heavily faulted zones. Higher TRI values also define Fe-mounds but at significantly smaller scales. The black outlines mark all mapped hydrothermal fields at Hatiba Mons, including confirmed and unconfirmed fields.

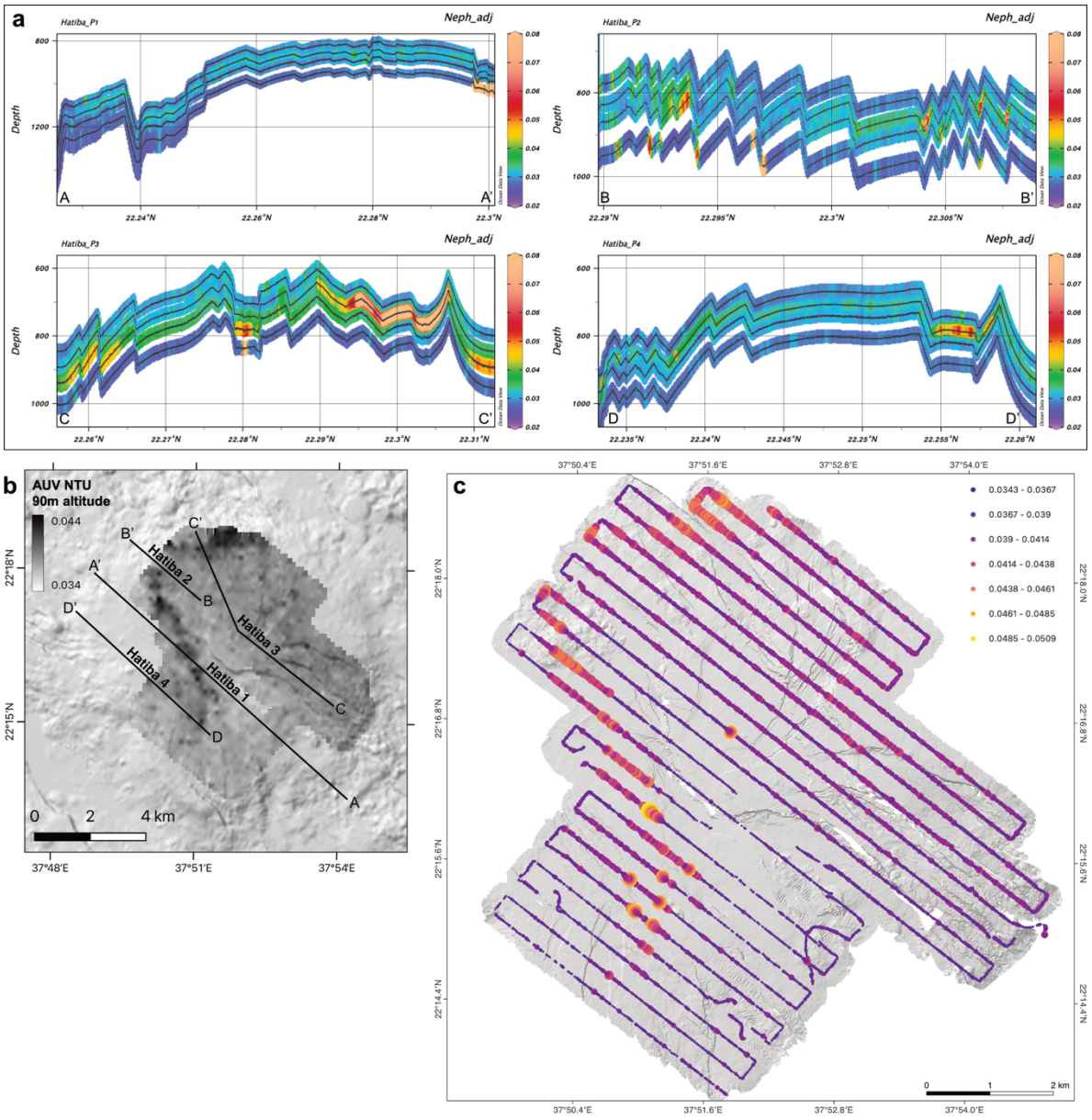

Supplementary Figure 2 - Turbidity anomalies at the Hatiba Mons volcano. **(a)** Visualization of MAPR tow-yo data (Miniature Autonomous Plume Recorder) measured in October/November 2021 (*RV Azizi*). Five MAPRs were mounted on the cable at an equal distance of 50 m. **(b)** Positions of the MAPR profiles shown in (a) and 150 m gridded turbidity anomalies at 90 m altitude from an AUV survey in February 2022 (*OSS Handin Tide*). **(c)** Detailed map of the AUV-derived turbidity anomalies, 90 m above ground over Hatiba Mons. The gaps in the track lines are due to failed merging of the processed AUV navigation with the raw turbidity data and therefore raw navigation was used instead. Since there are no significant signals within the affected areas, this does not disturb the overall turbidity pattern. Although measured in different months, all data (MAPR and AUV) reveal the most significant anomalies in the northern valley and at the western axial graben. However, the source of the turbidity anomalies remains unknown due to the lack of detailed bottom current data.

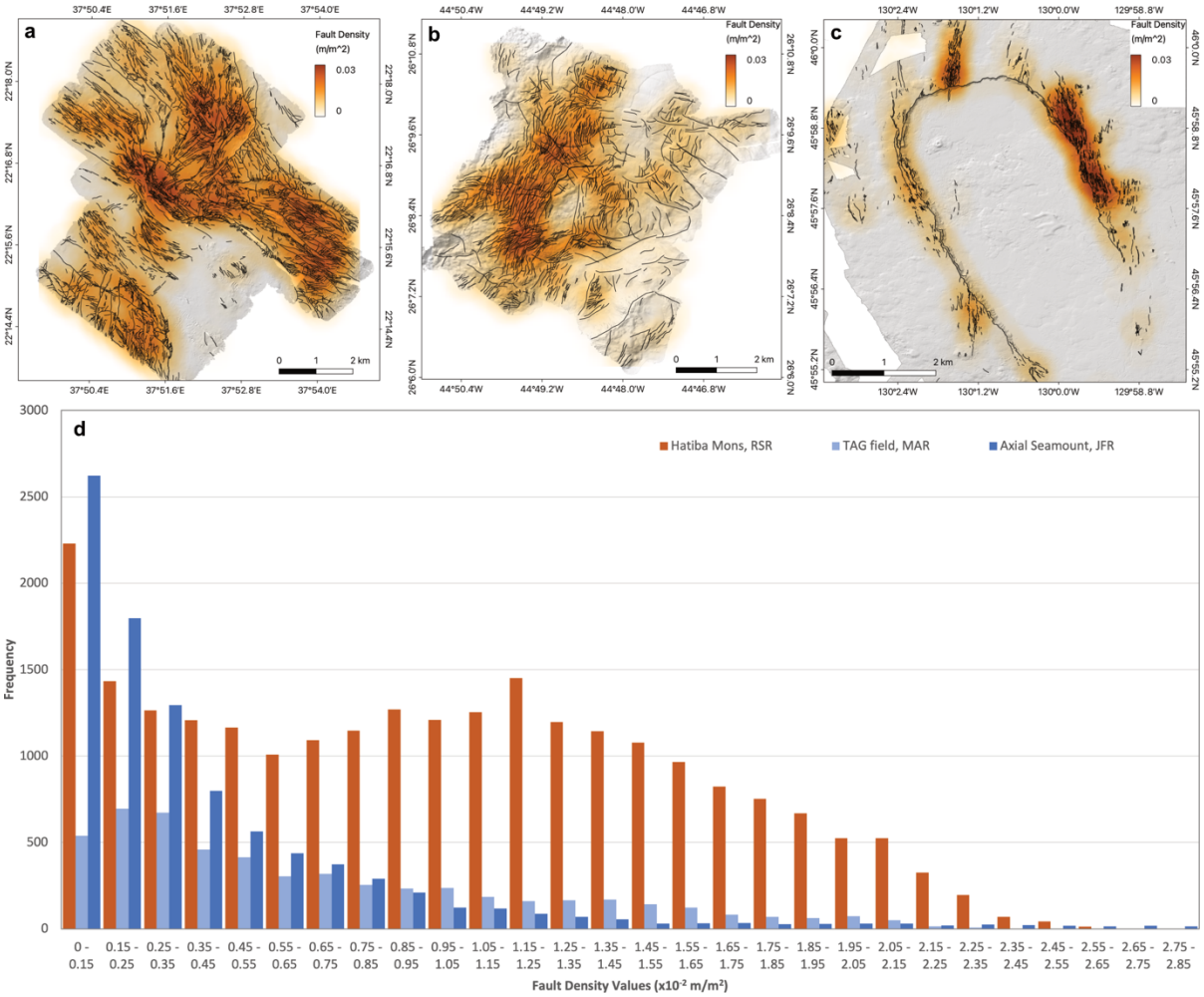

Supplementary Figure 3 - (a-c) Fault density maps of Hatiba Mons (Red Sea Rift, this study), the TAG Hydrothermal Field (Mid-Atlantic Ridge; Graber et al., 2020[1]), and Axial Volcano (Juan de Fuca Ridge; Clague et al., 2022[2]). The fault maps were derived from high-resolution (1–2 m) AUV bathymetry, and density was calculated with the *GDAL Line density* module in QGIS. The line density algorithm calculates the density of linear features in a circular neighborhood within a raster cell. The total lengths of all lines intersected by the search radius (set to r=500 m) are divided by the area. The line density's pixel size (cell size) was set to 100 m. The size of the search area per cell is 7.85×10^5 m^2 (r=500 m, $A=\pi \cdot r^2$). For example, a fault density value of 1×10^{-2} m/m^2 equals a summed-up fault and fissure length of 7.85 km within the search radius. **(d)** Fault density histograms from data of the above-shown areas. The histogram shows a significantly higher amount of high fault density areas at Hatiba Mons volcano compared to the two other mid-ocean ridge segments, known for the presence of several active and inactive high-T vent sites. This high number of faults and fissures, combined with the positive relief of the Hatiba Mons volcano, emphasizes a very effective cooling of the crust. In addition, larger parts (50%) of the surface of Hatiba Mons show a high fault density (>1 × 10-2 m/m2), when compared to TAG (25%) and Axial Seamount (<10%).

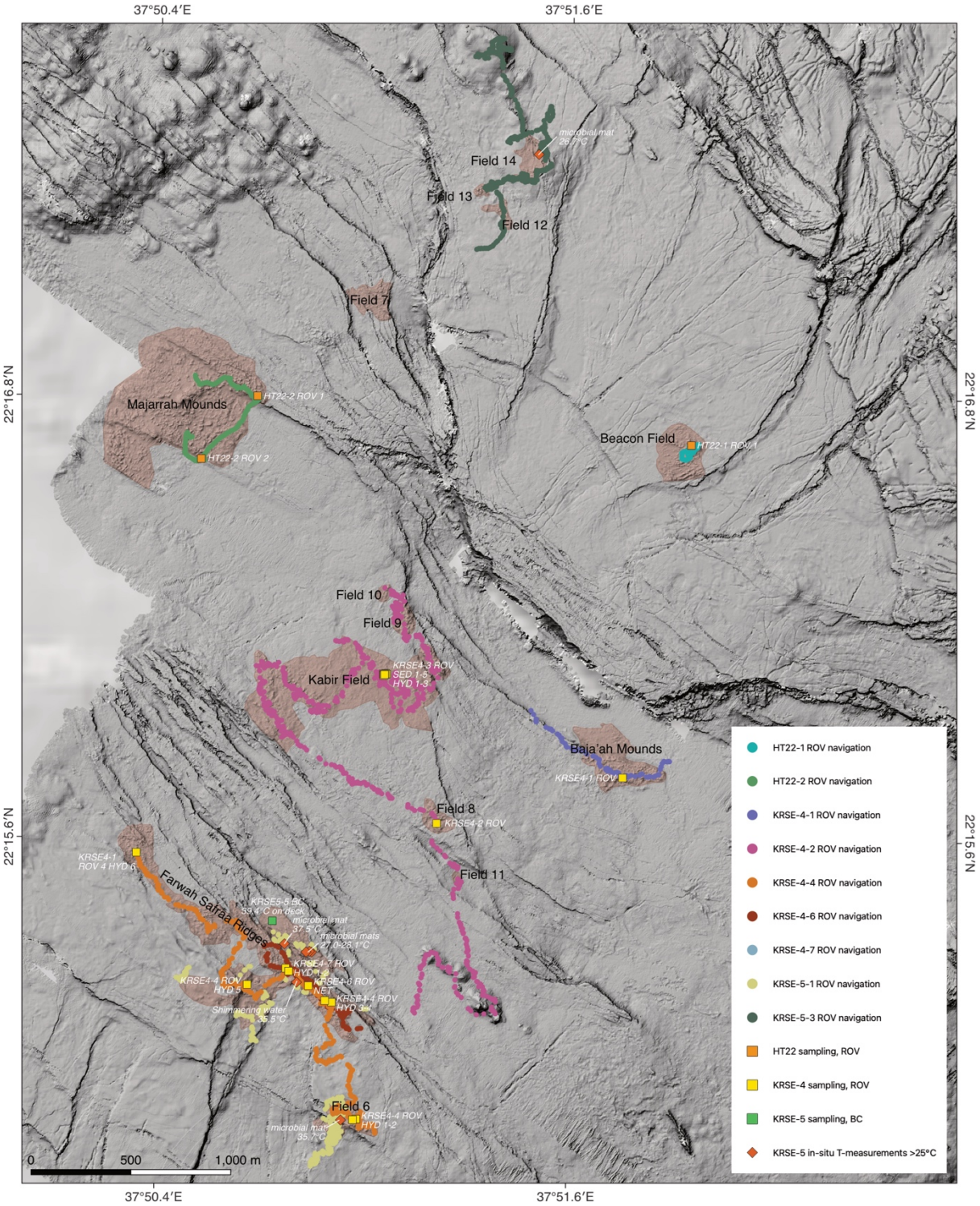

Supplementary Figure 4 - Track lines of ROV dives (color-coded lines) and sampling locations (yellow squares) of the 2022 campaigns superimposed on shaded AUV bathymetry of the Hatiba Mons summit area. Confirmed mound fields are marked pale-reddish. The USBL navigation accuracy in February 2022 was ±2 m, while the dives in May 2022 had an accuracy of ±50 m. Positions and temperatures of in-situ temperature measurements, with an untethered HOBO T-logger (see also Methods section), are also given in the map. HT22 = Fugro OSS Handin Tide cruise in 02/2022, KRSE-4 = KAUST Red Sea Expedition 4 in 05/2022 (RV Aegaeo), KRSE-5 = KAUST Red Sea Expedition 5 in 02/2023 (RV Aegaeo), ROV = Remotely Operated Vehicle, BC=Box Corer.

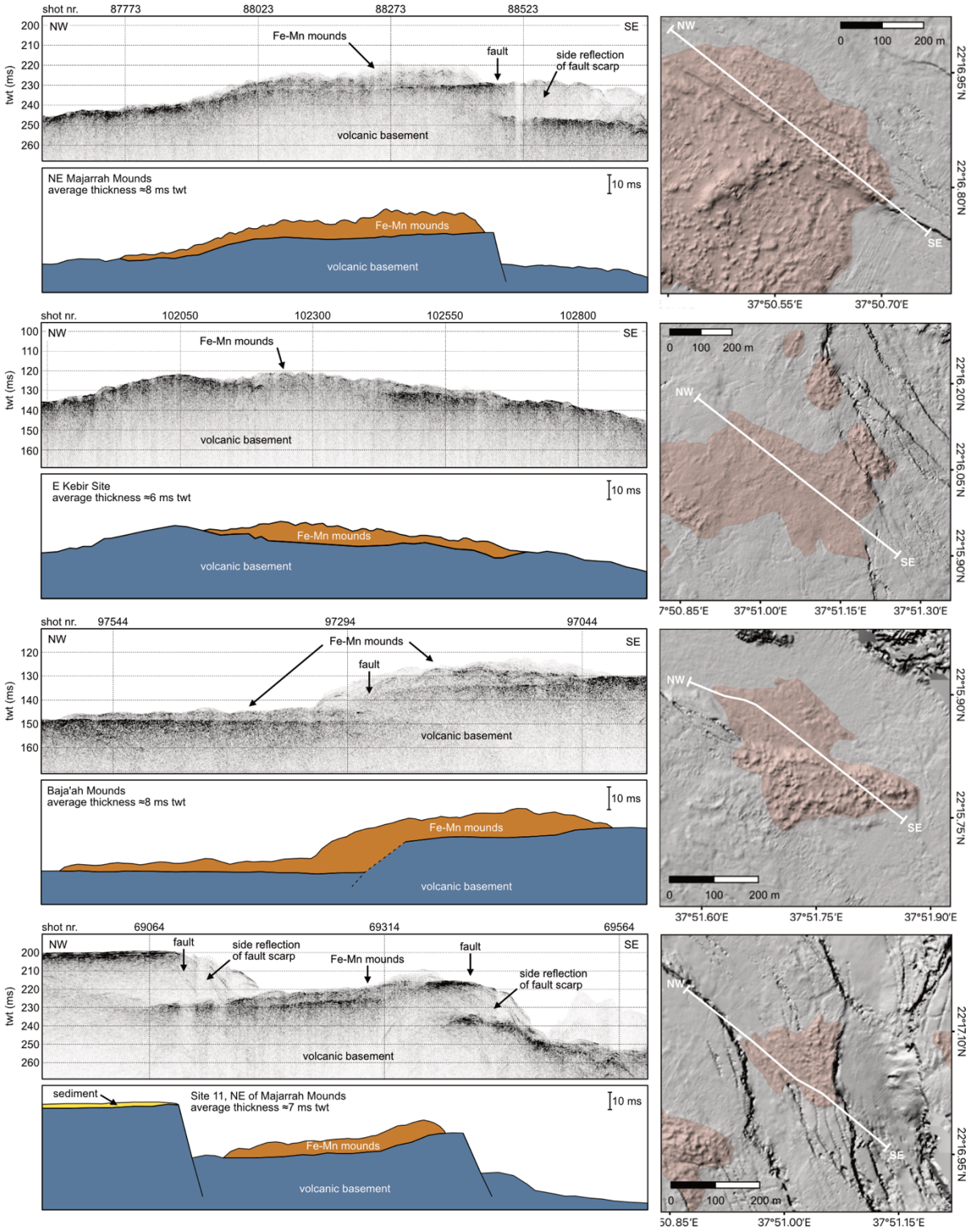

Supplementary Figure 5 - AUV sub-bottom profiles (SBP) and interpretations over several of the Fe-mound fields. The profiles show that the hydrothermal mounds lie on top of the basaltic basement with thicknesses of 6-8 m two-way-travel-time (twt), which equals 4.8–6.4 m (with an assumed sound velocity of 1600 m/s).

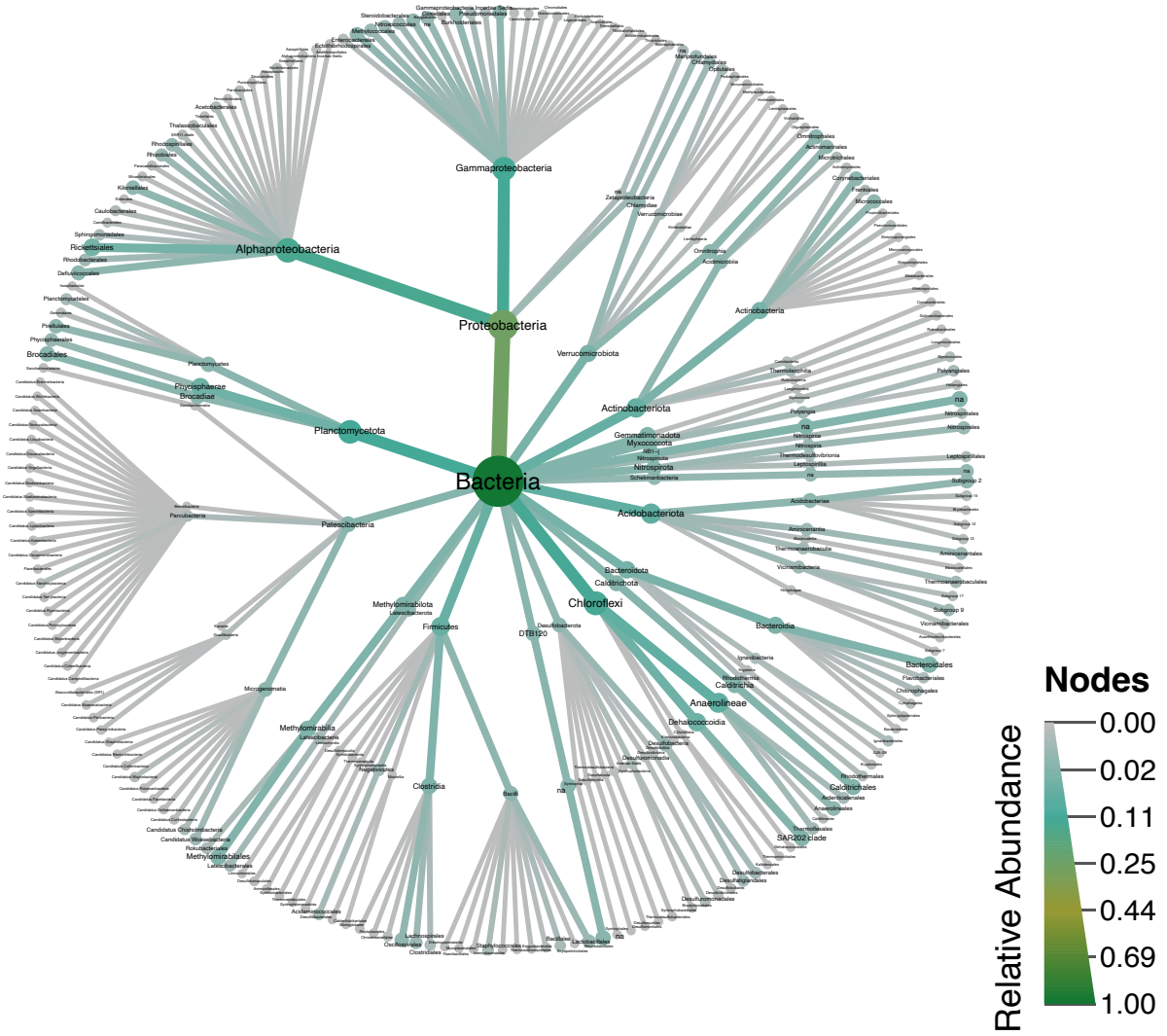

Supplementary Figure 6 - Dendrogram showing the relative abundance of the top twenty taxa at different ranks present in KRSE4-2 ROV, KRSE4-3 ROV, KRSE4-4 ROV, KRSE4-6 ROV samples obtained from 16S rRNA gene sequencing.

Supplementary Table 1: Sample locations

Sample name	Latitude (°N)	Longitude(°E)	Depth (m)	Hydrothermal field	Sample type
KRSE4-1 ROV HYD	22° 15.77	37° 51.76	1003	Baja'ah Mounds	Rock fragments from base type 1B chimney with microbes
KRSE4-2 ROV HYD	22° 15.64	37° 51.22	947	Field 8	Rock fragment from type 1A chimney with minor microbes
KRSE4-3 ROV HYD 1	22° 16.05	37° 51.06	960	Kabir Field	Type 1A chimney
KRSE4-3 ROV HYD 2	22° 16.05	37° 51.06	960	Kabir Field	Crust of mound side
KRSE4-3 ROV HYD 3	22° 16.05	37° 51.06	960	Kabir Field	Crust of mound side
KRSE4-3 ROV SED 1	22° 16.05	37° 51.06	960	Kabir Field	Sedimentary push core in type 3A mat
KRSE4-3 ROV SED 2	22° 16.05	37° 51.06	960	Kabir Field	Sedimentary push core in type 2A-3A mat
KRSE4-3 ROV SED 3	22° 16.05	37° 51.06	960	Kabir Field	Sedimentary push core in type 3B white patch
KRSE4-3 ROV SED 4	22° 16.05	37° 51.06	960	Kabir Field	Sedimentary push core in type 2A-3A mat
KRSE4-3 ROV SED 5	22° 16.05	37° 51.06	960	Kabir Field	Sedimentary push core in type 3B white patch
KRSE4-4 ROV HYD 1	22° 14.84	37° 50.99	897	Field 6	Crust of mound side
KRSE4-4 ROV HYD 2	22° 14.84	37° 50.98	896	Field 6	Crust of mound side
KRSE4-4 ROV HYD 3	22° 15.16	37° 50.91	890	Farwah Safraa ridges	Rock fragments of type 1A chimney
KRSE4-4 ROV HYD 4	22° 15.16	37° 50.89	887	Farwah Safraa ridges	Type 1A chimeny with microbes
KRSE4-4 ROV HYD 5	22° 15.20	37° 50.67	871	Farwah Safraa ridges	Rock fragments from base type 1A chimney
KRSE4-4 ROV HYD 6	22° 15.56	37° 50.34	858	Farwah Safraa ridges	Rock fragments of type 2A crust with microbes
KRSE4-4 ROV HYD X	undefined	undefined	undefined	Farwah Safraa ridges and field 6	Rock fragements from ROV dive 6 with undefined sample location
KRSE4-6 ROV NET	22° 15.20	37° 50.85	884	Farwah Safraa ridges	Microbial mat
KRSE4-7 ROV HYD 1	22° 15.25	37° 50.78	875	Farwah Safraa ridges	Type 2A chimney with microbes that displayed shimmering water venting
KRSE4-7 ROV HYD 2	22° 15.24	37° 50.79	875	Farwah Safraa ridges	Type 1B chimney with microbes
KRSE5-5 BC	22° 15.38	37° 50.74	897	Farwah Safraa ridges	Grainy green sediment with red patches at bottom
HT22-1 ROV 1	22°16.674'N	37°51.951'E	855	Beacon Field	Crust of mound side
HT22-2 ROV 1	22°16.800'N	37°50.685'E	949	Majarrah Mounds	Crust of mound side
HT22-2 ROV 2	22°16.629'N	37°50.523'E	973	Majarrah Mounds	Basalt from lava field

Supplementary Table 2: Mineralogy and Chemistry

Sample name	Rock type	XRD mineralogy
KRSE4-3 ROV HYD 1	Fe-oxyhydroxide (ochre)	x-ray amorph
KRSE4-3 ROV HYD 2A	Si-Fe oxyhydroxide (green)	x-ray amorph, nontronite
KRSE4-3 ROV HYD 2B	Fe-oxyhydroxide (ochre)	x-ray amorph
KRSE4-3 ROV HYD 1A	Fe-oxyhydroxide (ochre)	x-ray amorph
KRSE4-3 ROV HYD 1B	Fe-oxyhydroxide (ochre)	x-ray amorph
KRSE4-4 ROV HYD 2	Mn-oxide (black)	x-ray amorph
KRSE4-4 ROV HYD XA	Si-Fe oxyhydroxide (green, yellow-orange)	x-ray amorph, nontronite
KRSE4-4 ROV HYD XB	Mn-oxide (black)	x-ray amorph, todorokite, halite, quartz
KRSE4-4 ROV HYD XC	Si-Fe oxyhydroxide (green)	x-ray amorph, nontronite
KRSE4-7 ROV HYD 2A	Mn-oxide (black-red)	x-ray amorph, halite
KRSE4-7 ROV HYD 2B	Fe-oxyhydroxide (ochre)	x-ray amorph, halite
HT22-1 ROV 1	Mn-oxide (black)	x-ray amorph
HT22-2 ROV 1	Fe-oxyhydroxide (ochre)	x-ray amorph
Nod-P-1 Standard	Mn nodule	NA
HT22-2 ROV 2A	Basalt glass	NA
HT22-2 ROV 2B	Basalt glass	NA
HT22-2 ROV 2C	Basalt glass	NA
Average Red Sea (van der Zwan et al. 2015[3])	Basalt average	NA
StDev Red Sea		
Average Hatiba-Hadarba Deep (van der Zwan et al., 2015[3])	Basalt average	NA
StDev Hatiba-Hadarba Deep		

Supplementary Table 2: Mineralogy and Chemistry (*continued*)

Sample name	SiO_2 (%)	TiO_2 (%)	Al_2O_3 (%)	Fe_2O_3 (%)	MnO (%)	MgO (%)	CaO (%)	Na_2O (%)	K_2O (%)	P_2O_5 (%)
KRSE4-3 ROV HYD 1	16.28	<0.01	0.24	55.41	0.65	1.59	1.68	5.11	0.28	0.55
KRSE4-3 ROV HYD 2A	44.2	<0.01	0.01	40.01	0.08	2.5	0.3	2.06	2.61	0.09
KRSE4-3 ROV HYD 2B	13.6	0.03	0.39	43.77	3.3	2.14	10.12	2.94	0.31	0.64
KRSE4-3 ROV HYD 1A	19.11	<0.01	0.15	55.51	4.87	1.06	0.56	3	0.31	0.41
KRSE4-3 ROV HYD 1B	19.14	0.09	1.14	59.08	2.67	0.98	0.48	2.68	0.35	0.41
KRSE4-4 ROV HYD 2	20.66	0.26	2.52	15.7	23.23	4.47	9.21	2.5	1.1	0.13
KRSE4-4 ROV HYD XA	40.09	0.01	0.15	40.8	0.66	2.48	0.53	2.85	1.79	0.14
KRSE4-4 ROV HYD XB	3.84	0.03	0.78	7.53	31.82	5.39	17	2.53	0.84	0.17
KRSE4-4 ROV HYD XC	43.19	<0.01	0.06	39.55	0.19	2.66	0.51	2.62	2.1	0.11
KRSE4-7 ROV HYD 2A	12.3	0.02	0.26	26.45	29.61	2.52	2.06	5.06	0.71	0.23
KRSE4-7 ROV HYD 2B	22.38	0.01	0.16	47.54	0.89	1.29	1.29	6.22	0.47	0.33
HT22-1 ROV 1	31.65	0.05	0.54	28.53	17.09	3.04	0.91	3.01	1.71	0.17
HT22-2 ROV 1	18.66	0.02	0.34	45.77	3.95	2.38	7.46	2.27	0.61	0.47
Nod-P-1 Standard	14.42	0.45	4.68	8.36	37.85	3.32	3.00	2.21	1.21	0.46
HT22-2 ROV 2A	50.60	1.63	14.40	11.91	0.19	6.73	11.67	2.77	0.15	0.13
HT22-2 ROV 2B	50.44	1.64	14.32	11.88	0.19	6.75	11.59	2.80	0.15	0.11
HT22-2 ROV 2C	49.80	1.63	14.42	11.79	0.19	6.75	11.67	2.79	0.15	0.13
Average Red Sea	50.05	1.55	14.75	10.96	0.19	7.41	11.65	2.67	0.19	0.13
StDev Red Sea	*0.63*	*0.33*	*0.59*	*1.30*	*0.03*	*0.79*	*0.79*	*0.37*	*0.14*	*0.06*
Average Hatiba-Hadarba Deep	49.57	1.75	14.61	11.63	0.19	7.28	11.42	2.64	0.15	0.15
StDev Hatiba-Hadarba Deep	*0.27*	*0.22*	*0.23*	*0.57*	*0.02*	*0.47*	*0.45*	*0.13*	*0.03*	*0.03*

Supplementary Table 2: Mineralogy and Chemistry (*continued*)

Sample name	BaO (%)	Cr_2O_3 (%)	Cl (%)	F (%)	SO_3 (%)	Total (%)	LOI at 1000°C (%)	C (%)	S (%)	Li (ppm)
KRSE4-3 ROV HYD 1	<0.01	<0.01			0.93	107.2	19.01	0.6	0.26	<10
KRSE4-3 ROV HYD 2A	<0.01	<0.01			0.13	100.35	7.63	0.05	0.04	<10
KRSE4-3 ROV HYD 2B	<0.01	<0.01			0.51	101.2	20.7	2.1	0.15	20
KRSE4-3 ROV HYD 1A	0.02	<0.01			0.55	101.75	13.19	0.14	0.12	<10
KRSE4-3 ROV HYD 1B	0.01	<0.01			0.47	103.15	13.09	0.09	0.14	<10
KRSE4-4 ROV HYD 2	0.17	<0.01			0.36	102.2	18.72	1.61	0.1	70
KRSE4-4 ROV HYD XA	<0.01	<0.01			0.27	101.75	10.21	0.07	0.08	10
KRSE4-4 ROV HYD XB	0.13	<0.01			0.44	100.7	25.97	3.44	0.1	150
KRSE4-4 ROV HYD XC	<0.01	<0.01			0.22	101.55	8.86	0.06	0.05	10
KRSE4-7 ROV HYD 2A	0.04	<0.01			0.55	106.95	20.89	0.22	0.15	110
KRSE4-7 ROV HYD 2B	<0.01	<0.01			0.82	106.35	18.51	0.29	0.19	<10
HT22-1 ROV 1	0.04	<0.01			0.25	102.5	12.68	0.12	0.05	60
HT22-2 ROV 1	0.02	<0.01			0.44	101.65	16.98	1.52	0.14	10
Nod-P-1 Standard	0.3	<0.01			0.19	98	14.66	0.25	0.04	150
HT22-2 ROV 2A			0.02	0.08	0.31	100.27				
HT22-2 ROV 2B			0.02	0.05	0.29	99.94				
HT22-2 ROV 2C			0.02	0.08	0.30	99.42				
Average Red Sea			0.03							
StDev Red Sea			*0.03*							
Average Hatiba-Hadarba Deep			0.04							
StDev Hatiba-Hadarba Deep			*0.03*							

Supplementary Table 2: Mineralogy and Chemistry (*continued*)

Sample name	Sc (ppm)	V (ppm)	Cr (ppm)	Co (ppm)	Ni (ppm)	Cu (ppm)	Zn (ppm)	Ga (ppm)	Ge (ppm)	As (ppm)
KRSE4-3 ROV HYD 1	0.4	147	<5	3	2	2	21	0.9	5	126
KRSE4-3 ROV HYD 2A	0.2	6	<5	1	2	<1	9	0.3	11.6	9.6
KRSE4-3 ROV HYD 2B	1.2	215	6	4	14	6	53	2.2	3.1	136.5
KRSE4-3 ROV HYD 1A	0.6	203	5	33	39	11	149	2.3	4.2	139
KRSE4-3 ROV HYD 1B	1.5	114	8	24	13	11	129	2.3	3.9	68.9
KRSE4-4 ROV HYD 2	6.5	96	17	38	65	35	163	11.4	1	48.3
KRSE4-4 ROV HYD XA	0.5	18	<5	3	3	2	473	0.9	12	205
KRSE4-4 ROV HYD XB	0.8	108	<5	26	120	37	417	13	0.5	87.8
KRSE4-4 ROV HYD XC	0.2	11	<5	1	3	<1	329	1.1	29.5	192.5
KRSE4-7 ROV HYD 2A	0.7	27	<5	12	23	4	472	10.3	4.3	>250
KRSE4-7 ROV HYD 2B	0.5	12	<5	4	2	2	239	1.1	7	>250
HT22-1 ROV 1	0.5	33	7	2	15	6	44	7.3	57	20.6
HT22-2 ROV 1	0.9	289	7	32	23	9	1220	2.7	20.5	215
Nod-P-1 Standard	8.8	488	19	2200	>10000	>10000	1490	40.2	1.6	79.9

Supplementary Table 2: Mineralogy and Chemistry (*continued*)

Sample name	Se (ppm)	Rb (ppm)	Sr (ppm)	Y (ppm)	Zr (ppm)	Nb (ppm)	Mo (ppm)	Ag (ppm)	La (ppm)	Ce (ppm)
KRSE4-3 ROV HYD 1	0.6	1.4	234	14.3	2	0.17	48	<0.5	1.6	4
KRSE4-3 ROV HYD 2A	<0.2	43.8	69.3	6.9	1	<0.05	1	<0.5	0.6	1.2
KRSE4-3 ROV HYD 2B	0.6	2	1630	10.1	6	0.34	18	<0.5	1.5	2.8
KRSE4-3 ROV HYD 1A	0.7	1.6	135.5	40.5	4	0.07	147	<0.5	8.2	16.5
KRSE4-3 ROV HYD 1B	0.3	2.8	80.2	36.9	12	0.73	115	<0.5	7	13.3
KRSE4-4 ROV HYD 2	0.2	14.4	665	7.2	20	0.91	108	<0.5	1.9	3.9
KRSE4-4 ROV HYD XA	<0.2	30.5	109	6	1	<0.05	4	<0.5	0.7	1.5
KRSE4-4 ROV HYD XB	0.2	5.2	1225	3.8	11	0.52	175	<0.5	1.4	2.1
KRSE4-4 ROV HYD XC	<0.2	46.4	91.5	6.6	2	<0.05	1	<0.5	0.6	1.1
KRSE4-7 ROV HYD 2A	0.3	3.9	320	5.3	4	0.27	227	<0.5	0.8	1.4
KRSE4-7 ROV HYD 2B	0.2	3.6	237	4.1	2	0.19	11	<0.5	0.4	0.8
HT22-1 ROV 1	<0.2	23.7	207	3.7	10	0.48	173	<0.5	1.1	2.3
HT22-2 ROV 1	0.8	7.8	360	17.8	5	0.14	105	<0.5	2.2	3.7
Nod-P-1 Standard	0.8	23.9	637	92.4	269	20.5	555	<0.5	111.5	327

Supplementary Table 2: Mineralogy and Chemistry (*continued*)

Sample name	Cd (ppm)	In (ppm)	Sn (ppm)	Sb (ppm)	Te (ppm)	Cs (ppm)	Ba (ppm)	Pr (ppm)	Nd (ppm)
KRSE4-3 ROV HYD 1	1	<0.005	<0.5	2.28	0.02	0.02	54.1	0.54	3.3
KRSE4-3 ROV HYD 2A	0.5	<0.005	<0.5	0.29	<0.01	2.19	26.7	0.18	1.2
KRSE4-3 ROV HYD 2B	1.4	<0.005	<0.5	4.37	0.04	0.09	87.4	0.48	2.2
KRSE4-3 ROV HYD 1A	0.8	<0.005	<0.5	4.36	0.06	0.02	253	1.38	6.9
KRSE4-3 ROV HYD 1B	0.6	<0.005	<0.5	2.33	0.02	0.14	145.5	1.26	6.5
KRSE4-4 ROV HYD 2	0.5	0.012	<0.5	5.18	0.09	0.59	1740	0.53	2.9
KRSE4-4 ROV HYD XA	0.7	<0.005	<0.5	1.4	<0.01	2.12	35.9	0.2	1
KRSE4-4 ROV HYD XB	1.1	<0.005	<0.5	21.9	0.11	0.13	1140	0.25	1.4
KRSE4-4 ROV HYD XC	0.6	<0.005	<0.5	1.29	<0.01	3.12	16.3	0.17	1.1
KRSE4-7 ROV HYD 2A	0.8	<0.005	<0.5	4.93	0.02	0.1	307	0.16	0.9
KRSE4-7 ROV HYD 2B	0.8	<0.005	<0.5	0.24	0.02	0.18	75.5	0.07	0.5
HT22-1 ROV 1	<0.5	<0.005	<0.5	2.21	0.03	0.56	427	0.32	1.3
HT22-2 ROV 1	1.2	<0.005	<0.5	5.96	0.03	0.2	197.5	0.52	2
Nod-P-1 Standard	19.7	0.097	2.5	41.6	4.79	1.66	2480	32.4	143

Supplementary Table 2: Mineralogy and Chemistry (*continued*)

Sample name	Sm (ppm)	Eu (ppm)	Gd (ppm)	Tb (ppm)	Dy (ppm)	Ho (ppm)	Er (ppm)	Tm (ppm)	Yb (ppm)	Lu (ppm)
KRSE4-3 ROV HYD 1	0.66	0.24	1.49	0.21	1.7	0.36	1.02	0.14	0.8	0.17
KRSE4-3 ROV HYD 2A	0.31	0.11	0.45	0.11	0.57	0.13	0.5	0.1	0.32	0.07
KRSE4-3 ROV HYD 2B	0.4	0.12	0.89	0.16	0.94	0.22	0.75	0.12	0.6	0.12
KRSE4-3 ROV HYD 1A	1.06	0.29	2.73	0.3	1.78	0.5	1.48	0.17	0.68	0.14
KRSE4-3 ROV HYD 1B	0.94	0.35	2.65	0.3	1.92	0.5	1.36	0.15	0.74	0.15
KRSE4-4 ROV HYD 2	0.73	0.21	1.04	0.16	1.16	0.26	0.73	0.12	0.67	0.11
KRSE4-4 ROV HYD XA	0.25	0.08	0.32	0.07	0.49	0.11	0.4	0.05	0.23	0.05
KRSE4-4 ROV HYD XB	0.19	0.1	0.35	0.04	0.33	0.06	0.32	0.04	0.2	0.06
KRSE4-4 ROV HYD XC	0.3	0.1	0.55	0.1	0.62	0.16	0.45	0.07	0.31	0.02
KRSE4-7 ROV HYD 2A	0.36	0.07	0.27	0.05	0.47	0.1	0.32	0.06	0.33	0.06
KRSE4-7 ROV HYD 2B	0.08	0.03	0.08	0.02	0.14	0.04	0.19	0.03	0.15	0.03
HT22-1 ROV 1	0.19	0.09	0.34	0.05	0.3	0.05	0.26	0.02	0.16	0.02
HT22-2 ROV 1	0.59	0.27	1.42	0.19	1.28	0.32	1.02	0.13	0.5	0.12
Nod-P-1 Standard	34.3	6.81	30.4	4.76	25.8	4.76	13.55	1.96	12.25	2.06

Supplementary Table 2: Mineralogy and Chemistry (*continued*)

Sample name	Hf (ppm)	Ta (ppm)	W (ppm)	Re (ppm)	Hg (ppm)	Tl (ppm)	Pb (ppm)	Bi (ppm)	Th (ppm)	U (ppm)
KRSE4-3 ROV HYD 1	0.11	0.1	0.7	<0.001	0.017	0.15	<2	<0.01	0.06	6.53
KRSE4-3 ROV HYD 2A	0.05	0.1	0.6	<0.001	0.011	<0.02	<2	<0.01	<0.05	0.12
KRSE4-3 ROV HYD 2B	0.17	0.1	0.9	<0.001	0.022	0.5	4	<0.01	0.11	2.63
KRSE4-3 ROV HYD 1A	0.13	0.1	0.6	<0.001	0.009	1.6	4	<0.01	<0.05	8.48
KRSE4-3 ROV HYD 1B	0.4	0.1	<0.5	<0.001	0.007	0.55	3	0.01	0.28	8.47
KRSE4-4 ROV HYD 2	0.69	0.1	4.9	<0.001	0.012	4.19	25	0.01	0.3	1.2
KRSE4-4 ROV HYD XA	0.09	0.1	<0.5	0.001	0.44	0.2	107	<0.01	<0.05	0.72
KRSE4-4 ROV HYD XB	0.35	0.1	5.1	<0.001	0.015	12.25	30	0.01	0.18	1.57
KRSE4-4 ROV HYD XC	0.1	0.1	<0.5	<0.001	0.047	0.47	24	<0.01	<0.05	0.45
KRSE4-7 ROV HYD 2A	0.17	0.1	1.3	<0.001	0.023	11.35	27	<0.01	0.08	1.51
KRSE4-7 ROV HYD 2B	0.12	0.1	0.6	<0.001	0.027	0.22	<2	<0.01	0.08	1.13
HT22-1 ROV 1	0.27	0.1	1.7	<0.001	0.01	0.38	25	<0.01	0.16	0.85
HT22-2 ROV 1	0.11	0.1	1.4	<0.001	0.02	6.37	6	<0.01	0.09	6.49
Nod-P-1 Standard	4.12	0.4	59.5	<0.001	0.053	186	482	4.68	15.15	3.97

Supplementary Table 3: Hydrothermal vent field comparisons

	Rift	Location	Full Spreading Rate*	Depth (mbsl)	Nr. of Fields	Dimensions	Total Area (m2)
ultra-slow	**Red Sea Rift**	Hatiba Mons fields	ultra-slow, 12 mm/yr	840 - 1020	45 fields mapped (14 confirmed) within a survey area about 55 km2 (deposit covers ≈3% of survey area)	from ≈50m up to >1000m across	1,587,054
	Mohns Ridge	Trollveggen (Troll Wall)	ultra-slow, <15 mm/yr	550 - 600	3 fields/areas high-T area at 550m depth low-T area at 600m depth extinct area at 460m depth	area with high-T venting and extinct field about 1000x200m**; numerous Fe-mounds spread over an area of about 900x200m**; extinct area nearby with comparable sizes of the low-T area**	560,000
	SW Indian Ridge	37°47'S 49°39'E, west of the Gallieni transform fault	ultra-slow, 14-16 mm/yr	2750	na	na	na
	Gulf of Aden	Westernmost GoA at 11°58'N 43°40'E	ultra-slow, 16 mm/yr	≈1400	na	na	na
slow	**Mid-Atlantic Ridge**	TAG hydrothermal field	slow, 26 mm/yr	3400 - 3600	11 sites within a survey area of about 46km2	60m to 400m across	454,256
	Woodlark Basin	Western WB, Franklin Seamount	slow, 27 mm/yr	2160 - 2360	3 areas indicated	300x100m to 1700x200m**	495,560

Supplementary Table 3: Hydrothermal vent field comparisons (*continued*)

	Rift	Mound Sizes	activity, fluid T	Description	References
ultra-slow	**Red Sea Rift**	avg 3m, max 12m high, max 15-20m basal diameter, deposit thickness ≈5m	active, 39.4°C (in Farwah Saffraa field, ambient seawater T 21.7°C)	see main text	this study
	Mohns Ridge	up to "several-m-high", 2-3m**, "<0.5 m to several m across", up to 10m**	active, max 270°C venting; 7°C within Fe-mound (ambient -0.4°C)	high-T venting along a 1km long fault at 10 high-T vent sites; diffuse low-T hydrothermal fluids but no shimmering water, siliceous Fe-deposits with Fe-mounds composed of laminated yellow to brown amorphous FeOOH, local black oxidized Mn-phases, mounds vary in shape from thin flat-lying mats to higher mounds with chimney-like edifices; stratified mound structure of millimeters- to centimeters-thick laminated resembling microtextures of biogenic origin	Pedersen et al., 2010[4] Johannessen et al., 2017[5]
	SW Indian Ridge	na	active, "warm"	southern rift flank, low-T silica rich FeOOH samples collected with TV-grab from 2750m depth, no high-T precipitats	Peng et al., 2011[6]
	Gulf of Aden	na	active, T-anomaly in water cloumn 0.5°C	southern rift flank, "extensive" areas of diffuse low-T venting, FeOOH precipitates, no high-T venting, no or sulfides; no faunal aggregations around vent opening	Choukroune et al., 1988[7] Juniper et al., 1990[8]
slow	**Mid-Atlantic Ridge**	Fe-oxides on Mound 11: up to 5m, Shimmering mound (low-T sulfides): ≈20m; Shinkai mound (sulfides): 70m	active, max 360°C	sulfide abundant, Fe-oxides precipitatin is limited	Graber et al., 2020[1]
	Woodlark Basin	avg 1.5-2m, max 7m high, max 8-10m basal diameter	active, 20-30°C	basaltic andesite volcano, deposits at 2143–2366 m water depth, numerous actively venting oxyhydroxide chimneys and mounds	Lisitsyn et al., 1991[9] Boyd and Scott, 2001[10]

Supplementary Table 3: Hydrothermal vent field comparisons (*continued*)

slow	**Lau Basin**	Valu Fa Ridge sites	slow, 30 mm/yr	Hine Hina sites ≈1850 Vai Lilli field ≈1700 Mariner Field ≈1900	4 sampling sites	3 sites, km away Hine Hina, two sites of ≈250m Vai Lili field ≈500m Mariner Field ≈100m	325,940
	Mid-Atlantic Ridge	S-MAR ner 9°33'S, Liliput vent field	slow, 33 mm/yr	1500	1	numerous Fe-oxide occurrances spread over 1000x250m	250,000
intermediate	**Juan de Fuca Ridge**	Axial Seamount	intermediate, 60 mm/yr	1500	6 fields	na	na
	Galapagos Spreading Center, 86°W	Mounds Abyssal Hydrothermal Field	intermediate, 63 mm/yr	2700	>60 ridges within a survey area >220km2 (deposits ≈1% of survey area)	ridges are 20-50m wide, combined lenght ≈88km**	2,205,525
	East Pacific Rise, 21°N	Red Seamount	intermediate, 63 mm/yr	1900 - 2400	6 fields	300x200m to 800x350m**	616,541
fast	**East Pacific Rise, 13°N**	Seamount 5	fast, 91 mm/yr	1000 - 1200	4 fields	170m to 300x200m**	122,836

Notes

fast >80 mm/a, intermediate 50-80 mm/a, slow 20-50 mm/a), ultraslow <20 mm/a; after LaFemina (2015)[18]

*full spreading rates from Argus et al. (2011)[19], DeMets et al. (1994)[20]

**read from the given mapes and figures

Supplementary Table 3: Hydrothermal vent field comparisons (*continued*)

slow	**Lau Basin**	na	active, ≈40°C (Hine Hina)	Fe–Mn–Si oxide samples recovered with TV-grab at the Hine Hina (diffuse venting at 40°C) , the Vai Lili and the Mariner hydrothermal field, Vai Lili black smokers and diffuse discharge, maximum temperature of one TVG sample (Mariner field) was 37.7 °C, deposits formed either as the result of direct from Fe-oxidizing bacteria or of the passive reactions on the surface of microbes	Fouquet 1989[11] Takai et al. 2008[12] Sun et al., 2011[13]
	Mid-Atlantic Ridge	na, more crusts and sediments instead of individual mounds	active, 4.8-15.8°C	4 main sites (Lustrog, Main Liliput, Limtoc, Roman City) along the eastern flank of an axial volcanic ridge, diffuse venting, fauna visually dominated by small mussels and sponges, Main Lilliput site consists of abundant semi-lithified FeOOH crusts and cm-thick orange (rarely greenish) FeOOH precipitates around the sites	Haase et al., 2009[14]
intermediate	**Juan de Fuca Ridge**	~0.1–0.5 m	na	sulfide abundand, Fe-oxides precipitatin is limited, iron-oxide deposits are mound-like accretions to widespread blanket-type deposits in an average water depth of 1,500 m	Kennedy et al., 2003[15]
	Galapagos Spreading Center, 86°W	high	na	elongated ridges 20-30km south of-axis at GSC 86°W, conical in section and generally elongate in plan, encrusted with thick deposits of manganese oxide, ccur in several patches, rmound chains oriented parallel to the rift and fault-block terrain	Lonsdale, 1977[16]
	East Pacific Rise, 21°N	mounds up to 1m,, deposit thickness estimated to be about 1m	active, 10-15°C	seamount located on 0.6Ma old crust, near 21°N EPR, iron oxide deposits ver several low pillow cones, as patches on caldera floor and summit, small dm scaled mounds and chimneys, hollow linear Fe-Mn crust ridges with FeMn oxides and Nontronite	Alt et al., 1988[17]
fast	**East Pacific Rise, 13°N**	mounds up to 1m, deposit thicknes estimated to be at least 1m	inactive?, T 2°C above ambient in 50cm depth	seamount located on 0.9Ma old crust, 86km east of the EPRnear 13°N, hydrothermal iron deposits form continuous fields up to 700m2, orange to yellow knobby mounds with hollow cm scaled chimneys, mounds often aligned in rows, no fluid flow observed	Alt et al., 1988[17]

Supplementary Table 4: Hatiba Mons hydrothermal field details

Hydrothermal Field	central lat (°N)	central lon (°E)	average depth (m)	location on Hatiba Mons	max. dimensions (width x length)	total area (m^2)	average total thickness*	average mound hight (AUV grid)
Majarrah Mounds	22.280	37.841	965	central valley	900m x 690m	417,817	8ms twt, 6.4m	3.8m (n=67)
Kabir Field	22.267	37.849	950	central valley	1040m x 550m	308,775	6ms twt, 4.8m	3.7m (n=20)
Farwah Safraa ridges				W-fault zone		325,416	n.d.	3.4m (n=67)
North Farwah Safraa ridges	22.259	37.839	860	W-fault zone, NE Vallis Occidentalis	770m x 200m	-	-	-
South Farwah Safraa ridges	22.254	37.847	875	W-fault zone, W-Platform	895m x 660m	-	-	-
Baja'ah Mounds	22.263	37.862	1010	central valley	510m x 330m	80,315	8ms twt, 6.4m	3.0m (n=35)
Beacon Field	22.277	37.865	860	NE Platform, SW shoulder of Vallis Orientalis	280m x 280m	57,353	7ms twt, 5.6m	4.8m (n=26)
Field 6	22.247	37.849	890	east shoulder of Vallis Occidentalis	290m x 180m	35,289	n.d.	3.6m (n=11)
Field 7	22.284	37.851	950	central valley	210m x 180m	27,614	n.d.	2.2m (n=25)
Field 8	22.261	37.854	950	central valley	200m x 100m	16,897	n.d.	2.7m (n=10)
Field 9	22.270	37.852	970	central valley	170m x 110m	14,827	n.d.	1.9m (n=4)
Field 10	22.271	37.851	970	central valley	90m x 60m	4,584	n.d.	2.3m (n=9)
Field 11	22.258	37.855	965	central valley	80m x 40m	2,837	n.d.	<1m
Field 12	22.289	37.857	886	rim of NE Platform	100m x 180m	8,303	n.d.	2.3m (n=14)
Field 13	22.291	37.858	875	rim of NE Platform	140m x 230m	24,571	n.d.	2.5m (n=21)
Field 14	22.289	37.856	890	rim of NE Platform	55m x 75m	3,565	n.d.	3.2m (n=9)
Inferred fields (AUV, n=31)						*258,889*	n.d.	
Total						**1,587,054**		

* based on AUV sub-bottom profile data, calculated at 1600m/s

** based on average thickness of the hydrothermal field of 3m as indicated by AUV sub-bottom data

*** estimated from ROV video footage

Supplementary Table 4: Hatiba Mons hydrothermal field details (*continued*)

Hydrothermal Field	max. mound hight (AUV grid)	volume of hydrothermal deposit** (m^3)	appearance and major types of microbial mats	abundance of microbial mats on individual mounds (%)***	abundance of microbial mats in the entire field (%)***
Majarrah Mounds	12m	2,423,338	2B, 3A, 3B, 4	<20%	≈10%
Kabir Field	6m	1,790,893	1B, 2B, 3A, 3B, 4	<40%	≈5%
Farwah Safraa ridges	10m	1,887,414			
North Farwah Safraa ridges	-	-	1A, 2A, 2B, 3A	<5%	<1%
South Farwah Safraa ridges	-	-	1A, 2A, 2B, 3B	up to 100%	≈20%
Baja'ah Mounds	8m	465,826	1B	<40%	≈10%
Beacon Field	12m	332,650	2B, 3B	<5%	<1%
Field 6	10m	204,679	2A, 2B, 4	<5%	≈1%
Field 7	4.5m	160,163	n.d.	n.d.	n.d.
Field 8	4.5m	98,005	1B, 4	<5%	<1%
Field 9	3.5m	85,999	1A, 1B	<10%	≈5%
Field 10	3m	26,589	1A, 1B	<5%	≈3%
Field 11	<1m	16,453	1B, 3A, 3B	<5%	<1%
Field 12	4m	48,157	1A	1%	<1%
Field 13	10m	142,513	1A	<1%	<1%
Field 14	6m	20,678	1A, 1B, 2B	<5%	<1%
Inferred fields (AUV, n=31)		1618212			
Total		**9,321,569**			

Supplementary Table 5: Microbiological (NCBI) labels

Original expedition sample name	NCBI SRA accession	Study	Bioproject_ accession	Biosample_ accession	Sample_name (NCBI SRA)	Library_ID
KRSE4-2 ROV HYD	SRR22738876	SRP413057	PRJNA910929	SAMN32151258	Dive_2_Sample_1	Dive_2_Sample_1-R1
KRSE4-2 ROV HYD					Dive_2_Sample_1	Dive_2_Sample_1-R2
KRSE4-2 ROV HYD	SRR22738870	SRP413057	PRJNA910929	SAMN32151259	Dive_2_Sample_2	Dive_2_Sample_2-R1
KRSE4-2 ROV HYD					Dive_2_Sample_2	Dive_2_Sample_2-R2
KRSE4-2 ROV HYD	SRR22738859	SRP413057	PRJNA910929	SAMN32151260	Dive_2_Sample_3	Dive_2_Sample_3-R1
KRSE4-2 ROV HYD					Dive_2_Sample_3	Dive_2_Sample_3-R2
KRSE4-2 ROV HYD	SRR22738848	SRP413057	PRJNA910929	SAMN32151261	Dive_2_Sample_4	Dive_2_Sample_4_R1
KRSE4-2 ROV HYD					Dive_2_Sample_4	Dive_2_Sample_4_R2
KRSE4-2 ROV HYD	SRR22738836	SRP413057	PRJNA910929	SAMN32151262	Dive_2_Sample_5	Dive_2_Sample_5_R1
KRSE4-2 ROV HYD					Dive_2_Sample_5	Dive_2_Sample_5_R2
KRSE4-2 ROV HYD	SRR22738875	SRP413057	PRJNA910929	SAMN32151263	Dive_2_Sample_6	Dive_2_Sample_6_R1
KRSE4-2 ROV HYD					Dive_2_Sample_6	Dive_2_Sample_6_R2
KRSE4-2 ROV HYD	SRR22738874	SRP413057	PRJNA910929	SAMN32151264	Dive_2_Sample_7	Dive_2_Sample_7_R1
KRSE4-2 ROV HYD					Dive_2_Sample_7	Dive_2_Sample_7_R2
KRSE4-2 ROV HYD	SRR22738873	SRP413057	PRJNA910929	SAMN32151265	Dive_2_Sample_8	Dive_2_Sample_8_R1
KRSE4-2 ROV HYD					Dive_2_Sample_8	Dive_2_Sample_8_R2
KRSE4-2 ROV HYD	SRR22738872	SRP413057	PRJNA910929	SAMN32151266	Dive_2_Sample_9	Dive_2_Sample_9_R1
KRSE4-2 ROV HYD					Dive_2_Sample_9	Dive_2_Sample_9_R2
KRSE4-3 ROV SED 2	SRR22738871	SRP413057	PRJNA910929	SAMN32151267	Dive_3_Sample_1	Dive_3_Sample_1_R1
KRSE4-3 ROV SED 2					Dive_3_Sample_1	Dive_3_Sample_1_R2
KRSE4-3 ROV SED 2	SRR22738869	SRP413057	PRJNA910929	SAMN32151268	Dive_3_Sample_2	Dive_3_Sample_2_R1
KRSE4-3 ROV SED 2					Dive_3_Sample_2	Dive_3_Sample_2_R2
KRSE4-3 ROV SED 2	SRR22738868	SRP413057	PRJNA910929	SAMN32151269	Dive_3_Sample_3	Dive_3_Sample_3_R1
KRSE4-3 ROV SED 2					Dive_3_Sample_3	Dive_3_Sample_3_R2
KRSE4-3 ROV SED 1	SRR22738867	SRP413057	PRJNA910929	SAMN32151270	Dive_3_Sample_4	Dive_3_Sample_4_R1
KRSE4-3 ROV SED 1					Dive_3_Sample_4	Dive_3_Sample_4_R2

Supplementary Table 5: Microbiological (NCBI) labels (*continued*)

Original expedition sample name	Title	Filename
KRSE4-2 ROV HYD	Dive 2_sample 1 = biological replicate 1	Dive-2-Sample-1_S884_L002_R1_001.fastq.gz
KRSE4-2 ROV HYD	Dive 2_sample 1 = biological replicate 1	Dive-2-Sample-1_S884_L002_R2_001.fastq.gz
KRSE4-2 ROV HYD	Dive 2_ sample 1 = biological replicate 2	Dive-2-Sample-2_S885_L002_R1_001.fastq.gz
KRSE4-2 ROV HYD	Dive 2_ sample 1 = biological replicate 2	Dive-2-Sample-2_S885_L002_R2_001.fastq.gz
KRSE4-2 ROV HYD	Dive 2_sample 1 = biological replicate 3	Dive-2-Sample-3_S886_L002_R1_001.fastq.gz
KRSE4-2 ROV HYD	Dive 2_sample 1 = biological replicate 3	Dive-2-Sample-3_S886_L002_R2_001.fastq.gz
KRSE4-2 ROV HYD	Dive 2_sample 2 = biological replicate 1	Dive-2-Sample-4_S887_L002_R1_001.fastq.gz
KRSE4-2 ROV HYD	Dive 2_sample 2 = biological replicate 1	Dive-2-Sample-4_S887_L002_R2_001.fastq.gz
KRSE4-2 ROV HYD	Dive 2_sample 2 = biological replicate 2	Dive-2-Sample-5_S888_L002_R1_001.fastq.gz
KRSE4-2 ROV HYD	Dive 2_sample 2 = biological replicate 2	Dive-2-Sample-5_S888_L002_R2_001.fastq.gz
KRSE4-2 ROV HYD	Dive 2_sample 2 = biological replicate 3	Dive-2-Sample-6_S889_L002_R1_001.fastq.gz
KRSE4-2 ROV HYD	Dive 2_sample 2 = biological replicate 3	Dive-2-Sample-6_S889_L002_R2_001.fastq.gz
KRSE4-2 ROV HYD	Dive 2_sample 3 = biological replicate 1	Dive-2-Sample-7_S890_L002_R1_001.fastq.gz
KRSE4-2 ROV HYD	Dive 2_sample 3 = biological replicate 1	Dive-2-Sample-7_S890_L002_R2_001.fastq.gz
KRSE4-2 ROV HYD	Dive 2_sample 3 = biological replicate 2	Dive-2-Sample-8_S891_L002_R1_001.fastq.gz
KRSE4-2 ROV HYD	Dive 2_sample 3 = biological replicate 2	Dive-2-Sample-8_S891_L002_R2_001.fastq.gz
KRSE4-2 ROV HYD	Dive 2_sample 3 = biological replicate 3	Dive-2-Sample-9_S892_L002_R1_001.fastq.gz
KRSE4-2 ROV HYD	Dive 2_sample 3 = biological replicate 3	Dive-2-Sample-9_S892_L002_R2_001.fastq.gz
KRSE4-3 ROV SED 2	Dive 3_mat_sample 1 = biological replicate 1	Dive-3-Sample-1_S893_L002_R1_001.fastq.gz
KRSE4-3 ROV SED 2	Dive 3_mat_sample 1 = biological replicate 1	Dive-3-Sample-1_S893_L002_R2_001.fastq.gz
KRSE4-3 ROV SED 2	Dive 3_mat_sample 1 = biological replicate 2	Dive-3-Sample-2_S894_L002_R1_001.fastq.gz
KRSE4-3 ROV SED 2	Dive 3_mat_sample 1 = biological replicate 2	Dive-3-Sample-2_S894_L002_R2_001.fastq.gz
KRSE4-3 ROV SED 2	Dive 3_mat_sample 1 = biological replicate 3	Dive-3-Sample-3_S895_L002_R1_001.fastq.gz
KRSE4-3 ROV SED 2	Dive 3_mat_sample 1 = biological replicate 3	Dive-3-Sample-3_S895_L002_R2_001.fastq.gz
KRSE4-3 ROV SED 1	Dive 3_mat_sample 2 = biological replicate 1	Dive-3-Sample-4_S896_L002_R1_001.fastq.gz
KRSE4-3 ROV SED 1	Dive 3_mat_sample 2 = biological replicate 1	Dive-3-Sample-4_S896_L002_R2_001.fastq.gz

Supplementary Table 5: Microbiological (NCBI) labels (*continued*)

Original expedition sample name	NCBI SRA accession	Study	Bioproject_ accession	Biosample_ accession	Sample_name (NCBI SRA)	Library_ID
KRSE4-3 ROV SED 1	SRR22738865	SRP413057	PRJNA910929	SAMN32151271	Dive_3_Sample_5	Dive_3_Sample_5_R1
KRSE4-3 ROV SED 1					Dive_3_Sample_5	Dive_3_Sample_5_R2
KRSE4-3 ROV SED 1	SRR22738866	SRP413057	PRJNA910929	SAMN32151272	Dive_3_Sample_6	Dive_3_Sample_6_R1
KRSE4-3 ROV SED 1					Dive_3_Sample_6	Dive_3_Sample_6_R2
KRSE4-3 ROV SED 4	SRR22738864	SRP413057	PRJNA910929	SAMN32151273	Dive_3_Sample_7	Dive_3_Sample_7_R1
KRSE4-3 ROV SED 4					Dive_3_Sample_7	Dive_3_Sample_7_R2
KRSE4-3 ROV SED 4	SRR22738863	SRP413057	PRJNA910929	SAMN32151274	Dive_3_Sample_8	Dive_3_Sample_8_R1
KRSE4-3 ROV SED 4					Dive_3_Sample_8	Dive_3_Sample_8_R2
KRSE4-3 ROV SED 4	SRR22738862	SRP413057	PRJNA910929	SAMN32151275	Dive_3_Sample_9	Dive_3_Sample_9_R1
KRSE4-3 ROV SED 4					Dive_3_Sample_9	Dive_3_Sample_9_R2
KRSE4-3 ROV SED 2	SRR22738861	SRP413057	PRJNA910929	SAMN32151276	Dive_3_Sample_10	Dive_3_Sample_10_R1
KRSE4-3 ROV SED 2					Dive_3_Sample_10	Dive_3_Sample_10_R2
KRSE4-3 ROV SED 2	SRR22738860	SRP413057	PRJNA910929	SAMN32151277	Dive_3_Sample_11	Dive_3_Sample_11_R1
KRSE4-3 ROV SED 2					Dive_3_Sample_11	Dive_3_Sample_11_R2
KRSE4-3 ROV SED 2	SRR22738858	SRP413057	PRJNA910929	SAMN32151278	Dive_3_Sample_12	Dive_3_Sample_12_R1
KRSE4-3 ROV SED 2					Dive_3_Sample_12	Dive_3_Sample_12_R2
KRSE4-3 ROV SED 1	SRR22738857	SRP413057	PRJNA910929	SAMN32151279	Dive_3_Sample_13	Dive_3_Sample_13_R1
KRSE4-3 ROV SED 1					Dive_3_Sample_13	Dive_3_Sample_13_R2
KRSE4-3 ROV SED 1	SRR22738856	SRP413057	PRJNA910929	SAMN32151280	Dive_3_Sample_14	Dive_3_Sample_14_R1
KRSE4-3 ROV SED 1					Dive_3_Sample_14	Dive_3_Sample_14_R2
KRSE4-3 ROV SED 1	SRR22738854	SRP413057	PRJNA910929	SAMN32151281	Dive_3_Sample_15	Dive_3_Sample_15_R1
KRSE4-3 ROV SED 1					Dive_3_Sample_15	Dive_3_Sample_15_R2
KRSE4-3 ROV SED 4	SRR22738855	SRP413057	PRJNA910929	SAMN32151282	Dive_3_Sample_16	Dive_3_Sample_16_R1
KRSE4-3 ROV SED 4					Dive_3_Sample_16	Dive_3_Sample_16_R2
KRSE4-3 ROV SED 4	SRR22738853	SRP413057	PRJNA910929	SAMN32151283	Dive_3_Sample_17	Dive_3_Sample_17_R1
KRSE4-3 ROV SED 4					Dive_3_Sample_17	Dive_3_Sample_17_R2

Supplementary Table 5: Microbiological (NCBI) labels (*continued*)

Original expedition sample name	Title	Filename
KRSE4-3 ROV SED 1	Dive 3_mat_sample 2 = biological replicate 2	Dive-3-Sample-5_S897_L002_R1_001.fastq.gz
KRSE4-3 ROV SED 1	Dive 3_mat_sample 2 = biological replicate 2	Dive-3-Sample-5_S897_L002_R2_001.fastq.gz
KRSE4-3 ROV SED 1	Dive 3_mat_sample 2 = biological replicate 3	Dive-3-Sample-6_S898_L002_R1_001.fastq.gz
KRSE4-3 ROV SED 1	Dive 3_mat_sample 2 = biological replicate 3	Dive-3-Sample-6_S898_L002_R2_001.fastq.gz
KRSE4-3 ROV SED 4	Dive 3_mat_sample 3 = biological replicate 1	Dive-3-Sample-7_S899_L002_R1_001.fastq.gz
KRSE4-3 ROV SED 4	Dive 3_mat_sample 3 = biological replicate 1	Dive-3-Sample-7_S899_L002_R2_001.fastq.gz
KRSE4-3 ROV SED 4	Dive 3_mat_sample 3= biological replicate 2	Dive-3-Sample-8_S900_L002_R1_001.fastq.gz
KRSE4-3 ROV SED 4	Dive 3_mat_sample 3= biological replicate 2	Dive-3-Sample-8_S900_L002_R2_001.fastq.gz
KRSE4-3 ROV SED 4	Dive 3_mat_sample 3 = biological replicate 3	Dive-3-Sample-9_S901_L002_R1_001.fastq.gz
KRSE4-3 ROV SED 4	Dive 3_mat_sample 3 = biological replicate 3	Dive-3-Sample-9_S901_L002_R2_001.fastq.gz
KRSE4-3 ROV SED 2	Dive 3_sed_sample 1 = biological replicate 1	Dive-3-Sample-10_S902_L002_R1_001.fastq.gz
KRSE4-3 ROV SED 2	Dive 3_sed_sample 1 = biological replicate 1	Dive-3-Sample-10_S902_L002_R2_001.fastq.gz
KRSE4-3 ROV SED 2	Dive 3_sed_sample 1 = biological replicate 2	Dive-3-Sample-11_S903_L002_R1_001.fastq.gz
KRSE4-3 ROV SED 2	Dive 3_sed_sample 1 = biological replicate 2	Dive-3-Sample-11_S903_L002_R2_001.fastq.gz
KRSE4-3 ROV SED 2	Dive 3_sed_sample 1 = biological replicate 3	Dive-3-Sample-12_S904_L002_R1_001.fastq.gz
KRSE4-3 ROV SED 2	Dive 3_sed_sample 1 = biological replicate 3	Dive-3-Sample-12_S904_L002_R2_001.fastq.gz
KRSE4-3 ROV SED 1	Dive 3_sed_sample 2 = biological replicate 1	Dive-3-Sample-13_S905_L002_R1_001.fastq.gz
KRSE4-3 ROV SED 1	Dive 3_sed_sample 2 = biological replicate 1	Dive-3-Sample-13_S905_L002_R2_001.fastq.gz
KRSE4-3 ROV SED 1	Dive 3_sed_sample 2= biological replicate 2	Dive-3-Sample-14_S906_L002_R1_001.fastq.gz
KRSE4-3 ROV SED 1	Dive 3_sed_sample 2= biological replicate 2	Dive-3-Sample-14_S906_L002_R2_001.fastq.gz
KRSE4-3 ROV SED 1	Dive 3_sed_sample 2 = biological replicate 3	Dive-3-Sample-15_S907_L002_R1_001.fastq.gz
KRSE4-3 ROV SED 1	Dive 3_sed_sample 2 = biological replicate 3	Dive-3-Sample-15_S907_L002_R2_001.fastq.gz
KRSE4-3 ROV SED 4	Dive 3_sed_sample 3 = biological replicate 1	Dive-3-Sample-16_S908_L002_R1_001.fastq.gz
KRSE4-3 ROV SED 4	Dive 3_sed_sample 3 = biological replicate 1	Dive-3-Sample-16_S908_L002_R2_001.fastq.gz
KRSE4-3 ROV SED 4	Dive 3_sed_sample 3 = biological replicate 2	Dive-3-Sample-17_S909_L002_R1_001.fastq.gz
KRSE4-3 ROV SED 4	Dive 3_sed_sample 3 = biological replicate 2	Dive-3-Sample-17_S909_L002_R2_001.fastq.gz

Supplementary Table 5: Microbiological (NCBI) labels (*continued*)

Original expedition sample name	NCBI SRA accession	Study	Bioproject_ accession	Biosample_ accession	Sample_name (NCBI SRA)	Library_ID
KRSE4-3 ROV SED 4	SRR22738852	SRP413057	PRJNA910929	SAMN32151284	Dive_3_Sample_18	Dive_3_Sample_18_R1
KRSE4-3 ROV SED 4					Dive_3_Sample_18	Dive_3_Sample_18_R2
KRSE4-4 ROV HYD X	SRR22738851	SRP413057	PRJNA910929	SAMN32151285	Dive_4_Sample_1	Dive_4_Sample_1_R1
KRSE4-4 ROV HYD X					Dive_4_Sample_1	Dive_4_Sample_1_R2
KRSE4-4 ROV HYD X	SRR22738850	SRP413057	PRJNA910929	SAMN32151286	Dive_4_Sample_2	Dive_4_Sample_2_R1
KRSE4-4 ROV HYD X					Dive_4_Sample_2	Dive_4_Sample_2_R2
KRSE4-4 ROV HYD X	SRR22738849	SRP413057	PRJNA910929	SAMN32151287	Dive_4_Sample_3	Dive_4_Sample_3_R1
KRSE4-4 ROV HYD X					Dive_4_Sample_3	Dive_4_Sample_3_R2
KRSE4-6 ROV NET	SRR22738847	SRP413057	PRJNA910929	SAMN32151288	Dive_6_Sample_1	Dive_6_Sample_1_R1
KRSE4-6 ROV NET					Dive_6_Sample_1	Dive_6_Sample_1_R2
KRSE4-6 ROV NET	SRR22738846	SRP413057	PRJNA910929	SAMN32151289	Dive_6_Sample_2	Dive_6_Sample_2_R1
KRSE4-6 ROV NET					Dive_6_Sample_2	Dive_6_Sample_2_R2
KRSE4-6 ROV NET	SRR22738845	SRP413057	PRJNA910929	SAMN32151290	Dive_6_Sample_3	Dive_6_Sample_3_R1
KRSE4-6 ROV NET					Dive_6_Sample_3	Dive_6_Sample_3_R2
KRSE4-6 ROV NET	SRR22738843	SRP413057	PRJNA910929	SAMN32151291	Dive_6_Sample_4	Dive_6_Sample_4_R1
KRSE4-6 ROV NET					Dive_6_Sample_4	Dive_6_Sample_4_R2
KRSE4-6 ROV NET	SRR22738844	SRP413057	PRJNA910929	SAMN32151292	Dive_6_Sample_5	Dive_6_Sample_5_R1
KRSE4-6 ROV NET					Dive_6_Sample_5	Dive_6_Sample_5_R2
KRSE4-6 ROV NET	SRR22738842	SRP413057	PRJNA910929	SAMN32151293	Dive_6_Sample_6	Dive_6_Sample_6_R1
KRSE4-6 ROV NET					Dive_6_Sample_6	Dive_6_Sample_6_R2
KRSE4-6 ROV NET	SRR22738841	SRP413057	PRJNA910929	SAMN32151294	Dive_6_Sample_7	Dive_6_Sample_7_R1
KRSE4-6 ROV NET					Dive_6_Sample_7	Dive_6_Sample_7_R2
KRSE4-6 ROV NET	SRR22738840	SRP413057	PRJNA910929	SAMN32151295	Dive_6_Sample_8	Dive_6_Sample_8_R1
KRSE4-6 ROV NET					Dive_6_Sample_8	Dive_6_Sample_8_R2

Supplementary Table 5: Microbiological (NCBI) labels (*continued*)

Original expedition sample name	Title	Filename
KRSE4-3 ROV SED 4	Dive 3_sed_sample 3= biological replicate 3	Dive-3-Sample-18_S910_L002_R1_001.fastq.gz
KRSE4-3 ROV SED 4	Dive 3_sed_sample 3= biological replicate 3	Dive-3-Sample-18_S910_L002_R2_001.fastq.gz
KRSE4-4 ROV HYD X	Dive 4_sample 1 = biological replicate 1	Dive-4-Sample-1_S911_L002_R1_001.fastq.gz
KRSE4-4 ROV HYD X	Dive 4_sample 1 = biological replicate 1	Dive-4-Sample-1_S911_L002_R2_001.fastq.gz
KRSE4-4 ROV HYD X	Dive 4_sample 1 = biological replicate 2	Dive-4-Sample-2_S912_L002_R1_001.fastq.gz
KRSE4-4 ROV HYD X	Dive 4_sample 1 = biological replicate 2	Dive-4-Sample-2_S912_L002_R2_001.fastq.gz
KRSE4-4 ROV HYD X	Dive 4_sample 1= biological replicate 3	Dive-4-Sample-3_S913_L002_R1_001.fastq.gz
KRSE4-4 ROV HYD X	Dive 4_sample 1= biological replicate 3	Dive-4-Sample-3_S913_L002_R2_001.fastq.gz
KRSE4-6 ROV NET	Dive 6_sample 1 = biological replicate 1	Dive-6-Sample-1_S914_L002_R1_001.fastq.gz
KRSE4-6 ROV NET	Dive 6_sample 1 = biological replicate 1	Dive-6-Sample-1_S914_L002_R2_001.fastq.gz
KRSE4-6 ROV NET	Dive 6_sample 1 = biological replicate 2	Dive-6-Sample-2_S915_L002_R1_001.fastq.gz
KRSE4-6 ROV NET	Dive 6_sample 1 = biological replicate 2	Dive-6-Sample-2_S915_L002_R2_001.fastq.gz
KRSE4-6 ROV NET	Dive 6_sample 1= biological replicate 3	Dive-6-Sample-3_S916_L002_R1_001.fastq.gz
KRSE4-6 ROV NET	Dive 6_sample 1= biological replicate 3	Dive-6-Sample-3_S916_L002_R2_001.fastq.gz
KRSE4-6 ROV NET	Dive 6_sample 2= biological replicate 1	Dive-6-Sample-4_S917_L002_R1_001.fastq.gz
KRSE4-6 ROV NET	Dive 6_sample 2= biological replicate 1	Dive-6-Sample-4_S917_L002_R2_001.fastq.gz
KRSE4-6 ROV NET	Dive 6_sample 2= biological replicate 2	Dive-6-Sample-5_S918_L002_R1_001.fastq.gz
KRSE4-6 ROV NET	Dive 6_sample 2= biological replicate 2	Dive-6-Sample-5_S918_L002_R2_001.fastq.gz
KRSE4-6 ROV NET	Dive 6_sample 2= biological replicate 3	Dive-6-Sample-6_S919_L002_R1_001.fastq.gz
KRSE4-6 ROV NET	Dive 6_sample 2= biological replicate 3	Dive-6-Sample-6_S919_L002_R2_001.fastq.gz
KRSE4-6 ROV NET	Dive 6_sample 2= biological replicate 4	Dive-6-Sample-7_S920_L002_R1_001.fastq.gz
KRSE4-6 ROV NET	Dive 6_sample 2= biological replicate 4	Dive-6-Sample-7_S920_L002_R2_001.fastq.gz
KRSE4-6 ROV NET	Dive 6_sample 2= biological replicate 5	Dive-6-Sample-8_S921_L002_R1_001.fastq.gz
KRSE4-6 ROV NET	Dive 6_sample 2= biological replicate 5	Dive-6-Sample-8_S921_L002_R2_001.fastq.gz

Supplementary References

1. Graber, S. *et al.* Structural Control, Evolution, and Accumulation Rates of Massive Sulfides in the TAG Hydrothermal Field. *Geochemistry Geophysics Geosystems* **21**, 389–25 (2020).
2. Clague, D.A. *et al*. High-resolution AUV mapping and targeted ROV observations of three historical lava flows at Axial Seamount. *Oceanography*, **30**, 82-99 (2017).
3. van der Zwan, F.M. *et al.* Hydrothermal activity at the ultraslow- to slow-spreading Red Sea Rift traced by chlorine in basalt. *Chemical Geology* **405**, 63-81 (2015).
4. Pedersen, R. B. et al. Hydrothermal Activity at the Arctic Mid-Ocean Ridges. in Diversity of Hydrothermal Systems on Slow Spreading Ocean Ridges 67–89 (American Geophysical Union, 2010). doi:10.1029/2008gm000783.
5. Johannessen, K. C. *et al.* Environmental controls on biomineralization and Fe-mound formation in a low-temperature hydrothermal system at the Jan Mayen Vent Fields. *Geochim Cosmochim Ac* **202**, 101–123 (2017).
6. Peng, X. *et al.* Diversity of biogenic minerals in low-temperature Si-rich deposits from a newly discovered hydrothermal field on the ultraslow spreading Southwest Indian Ridge. *J Geophys Res Biogeosciences* **116**, (2011).
7. Choukroune, P. *et al.* Tectonics of an incipient oceanic rift. *Mar Geophys Res* **9**, 147–163 (1988).
8. Juniper, S. K., Tunnicliffe, V. & Desbruyères, D. Regional-Scale Features of Northeast Pacific, East Pacific Rise, and Gulf of Aden Vent Communities. in *Gorda Ridge, A Seafloor Spreading Center in the United States' Exclusive Economic Zone* (ed. McMurray, G. R.) 265–278 (Springer, 1990). doi:10.1007/978-1-4612-3258-2_19.
9. Lisitsyn, A. P. *et al.* Active hydrothermal activity at Franklin Seamount, Western Woodlark Sea (Papua New Guinea). *Int Geol Rev* **33**, 914–929 (1991).
10. Boyd, T. & Scott, S. Microbial and hydrothermal aspects of ferric oxyhydroxides and ferrosic hydroxides: the example of Franklin Seamount, Western Woodlark Basin, Papua New Guinea. *Geochem T* **2**, 45 (2001).
11. Fouquet, Y. & Stackelberg, U. von. *NAUTILAU French-German Diving Cruise with Nautile April 17 - May 10 1989*. (1989).
12. Takai, K. *et al.* Variability in the microbial communities and hydrothermal fluid chemistry at the newly discovered Mariner hydrothermal field, southern Lau Basin. *Journal of Geophysical Research* **113**, (2008).
13. Sun, Z. *et al.* Hydrothermal Fe–Si–Mn oxide deposits from the Central and South Valu Fa Ridge, Lau Basin. *Appl Geochem* **26**, 1192–1204 (2011).
14. Haase, K. M. *et al.* Diking, young volcanism and diffuse hydrothermal activity on the southern Mid-Atlantic Ridge: The Lilliput field at 9°33'S. *Marine Geology* **266**, 52–64 (2009).
15. Kennedy, C. B., Scott, S. D. & Ferris, F. G. Characterization of Bacteriogenic Iron Oxide Deposits from Axial Volcano, Juan de Fuca Ridge, Northeast Pacific Ocean. *Geomicrobiol J* **20**, 199–214 (2003).
16. Lonsdale, P. Deep-tow observations at the mounds abyssal hydrothermal field, Galapagos Rift. *Earth Planet Sc Lett* **36**, 92–110 (1977).
17. Alt, J. C. Hydrothermal oxide and nontronite deposits on seamounts in the eastern Pacific. *Mar Geol* **81**, 227–239 (1988).
18. LaFemina, P. C. The Encyclopedia of Volcanoes (Second Edition). *Part : Orig. Transp. Magma* 65–92 (2015) doi:10.1016/b978-0-12-385938-9.00003-1.
19. Argus, D. F., Gordon, R. G. & DeMets, C. Geologically current motion of 56 plates relative to the no-net-rotation reference frame. *Geochemistry Geophysics Geosystems* **12**, (2011).
20. DeMets, C., Gordon, R. G., Argus, D. F. & Stein, S. Effect of recent revisions to the geomagnetic reversal time scale on estimates of current plate motions. *Geophys Res Lett* **21**, 2191–2194 (1994).